Precise location of unsurveyed seamounts in the Austral archipelago area using SEASAT data

N. Baudry[*†], M. Diament[*] and Y. Albouy[†]

[*] *Laboratoire de Géophysique, U.A. du C.N.R.S. 730, Université Paris-Sud, 91405 Orsay Cedex, France*
[†] *ORSTOM, 213 rue Lafayette, 75481 Paris Cedex 10, France*

Summary. SEASAT altimetric geoid data are used to detect uncharted seamounts in the Austral archipelago area. The various physical parameters which affect the geoid signature of a seamount are inspected to analyse their influence on the precision of the location. These parameters are the shape of the seamount, its density, the crustal model, the effective elastic thickness of the lithosphere and the distance between the seamount and sub-satellite tracks, respectively. The results of the tests performed on synthetic data as well as on charted structures show that when a seamount is detected on at least two neighbouring tracks, it is possible to locate it with good confidence and to give an estimation of its height. If the correct elastic thickness is assumed, the precision on the location is order 15 km. Ten previously unsurveyed seamounts have been located in the Austral archipelago. It appears that they are emplaced along two well-defined azimuths (N 110°E and N 150°E) and that two parallel distinct volcanic chains form the Austral archipelago.

Key words: seamount location, SEASAT, Austral archipelago

Introduction

The intense coverage of the world oceans by satellite altimetry has provided a large amount of data in oceans which were previously very poorly covered with traditional marine measurements. It is well known that the short-wavelength ($\lambda < 400$ km) anomalies observed in the gravity field over the oceans are related to the bathymetric features and to the way they are isostatically supported. Therefore, several previous studies have been carried out in order to predict unknown bathymetry using the geoid anomalies as measured by satellites. These studies dealt with any kind of bathymetry (Dixon & Parke 1983; Watts *et al.* 1985a) or were devoted to a specific type of structure, including the fracture zone or linear features

(Sailor & Okal 1983; Sandwell 1984a; Okal & Cazenave 1985), and unknown seamounts (Lambeck & Coleman 1982; Lazarewicz & Schwank 1982; White *et al.* 1983; Sandwell 1984a). In these last studies, various prediction techniques were used in order to detect and locate seamounts. Lambeck & Coleman (1982) modelled seamount signatures visually detected on GEOS-3 or SEASAT profiles while Lazarewicz & Schwank (1982) and White *et al.* (1983) used matched filters applied to SEASAT data tracks. The location uncertainties, when given, appear to be good along-track (from 1.1 km to about 15 km) but much worse cross-track (25 km to more than 40 km). Sandwell (1984a) reveals the existence of 72 uncharted seamounts by examining a sea-surface image constructed from deflection of the vertical. The location uncertainty is then of about 50 km. Generally, no indication was given as to the heights of the seamounts. In fact, as pointed out by Watts & Ribe (1984), since most of the above-mentioned authors did not attempt to predict the height of uncharted seamounts, they generally neglected such important parameters as the tectonic setting, the dimensionality, the density of the topographic material, the depth of the isostatic compensation or the crustal structure. Therefore they only provided 'possible' locations of seamounts without any indication of shape. Precise location of uncharted seamounts is of major interest in poorly surveyed areas. Such a situation holds in the Austral archipelago in the South Central Pacific (Fig. 1), whose origin is commonly attributed to a hotspot presently located under the MacDonald submarine volcano (Morgan 1972). Nevertheless, some petrological evidence (see, for example Duncan & McDougall 1976) and the existence of two apparently distinct volcanic lineaments, MacDonald-to-Neilson and President Thiers Bank-to-Rurutu Islands (Jarrard & Clague 1977; Barsczus 1980; Barsczus & Liotard 1985), seem to demonstrate that this postulated single hotspot cannot account for all the features of the archipelago. New precise bathymetric information is necessary both to understand the geodynamic evolution of this area and as a guide for future geophysical cruises.

In the present paper we propose a method of location based on the interpretation of seamount signatures detected on SEASAT tracks in order to: (1) precisely locate the sea-mounts, i.e. with a minimum uncertainty both along-track and cross-track; and (2) give an
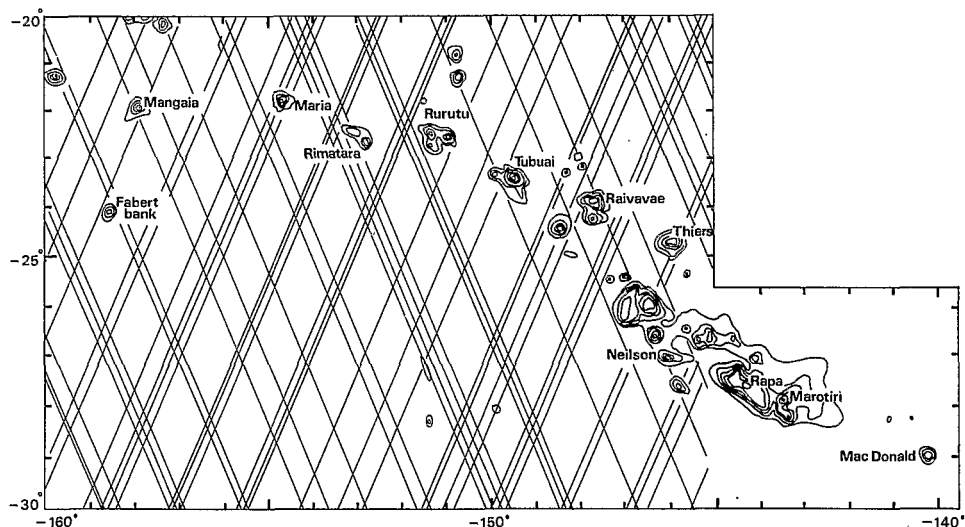

Figure 1. Known bathymetry in the Austral archipelago as inferred from the GEBCO charts. The SEASAT tracks are superimposed upon the area under study.
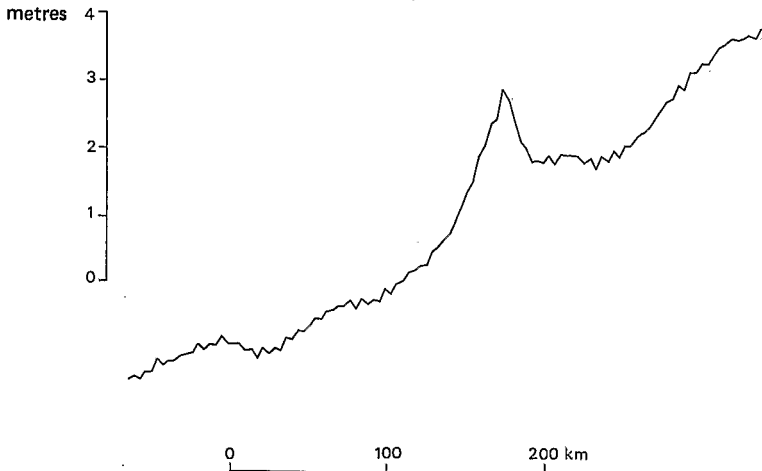
Figure 2. Typical SEASAT altimetric geoid over a seamount.

estimation of the size and the shape of the seamounts. For that purpose, we first present the results of an investigation of the effects of various parameters which affect the ability to locate and determine the shape of seamounts using first synthetic data and then SEASAT data. We then discuss the geodynamic implications of our results in the Austral archipelago area.

Geoid signature over a seamount

A typical altimetric profile over a seamount (Fig. 2) consists of a small anomaly super-imposed on a broad regional anomaly. Prior to a study of the seamount signature itself it is necessary to remove the long-wavelength geoid. This can be done using various approaches; for instance, subtracting some harmonics of a global geopotential field as given by models such as GRIM 3 (Reigber *et al.* 1983), or by removing either a polynomial curve or a straight line from the geoid anomaly over the seamount. Since the seamount signature is a short-wavelength anomaly, all these methods yield essentially identical results. Therefore, we chose to remove a straight line from the SEASAT data.

   The geoid signature over a seamount is the sum of a positive anomaly due to the excess bathymetry and of a negative anomaly due to the deflected crust beneath the structure (Fig. 3). The positive anomaly is controlled by the contrast between the mean density of the seamount and the seawater density, and by the morphology of the seamount. The negative anomaly is controlled by the contrast between the crustal density and the upper-mantle density, and by the depth and the shape of the Moho discontinuity. If the crust is divided into several layers, the negative anomaly would be a sum of all the anomalies due to the various density interfaces which are assumed to be deflected parallel to the Moho (Fig. 4). Since the negative anomaly (Fig. 3d) has a small amplitude and a larger wavelength than the positive anomaly (Fig. 3c), the total resulting anomaly (Fig. 3e) is reduced in amplitude with respect to the anomaly due to topography alone and presents a small negative trough all around the seamount. Such a trough is also theoretically present in the bathymetry but is generally masked by sediment infilling. The resulting geoid anomaly is wider than the bathymetric feature and it will be possible to detect and to locate a seamount *a priori* even if the altimetric track does not pass immediately above the seamount.
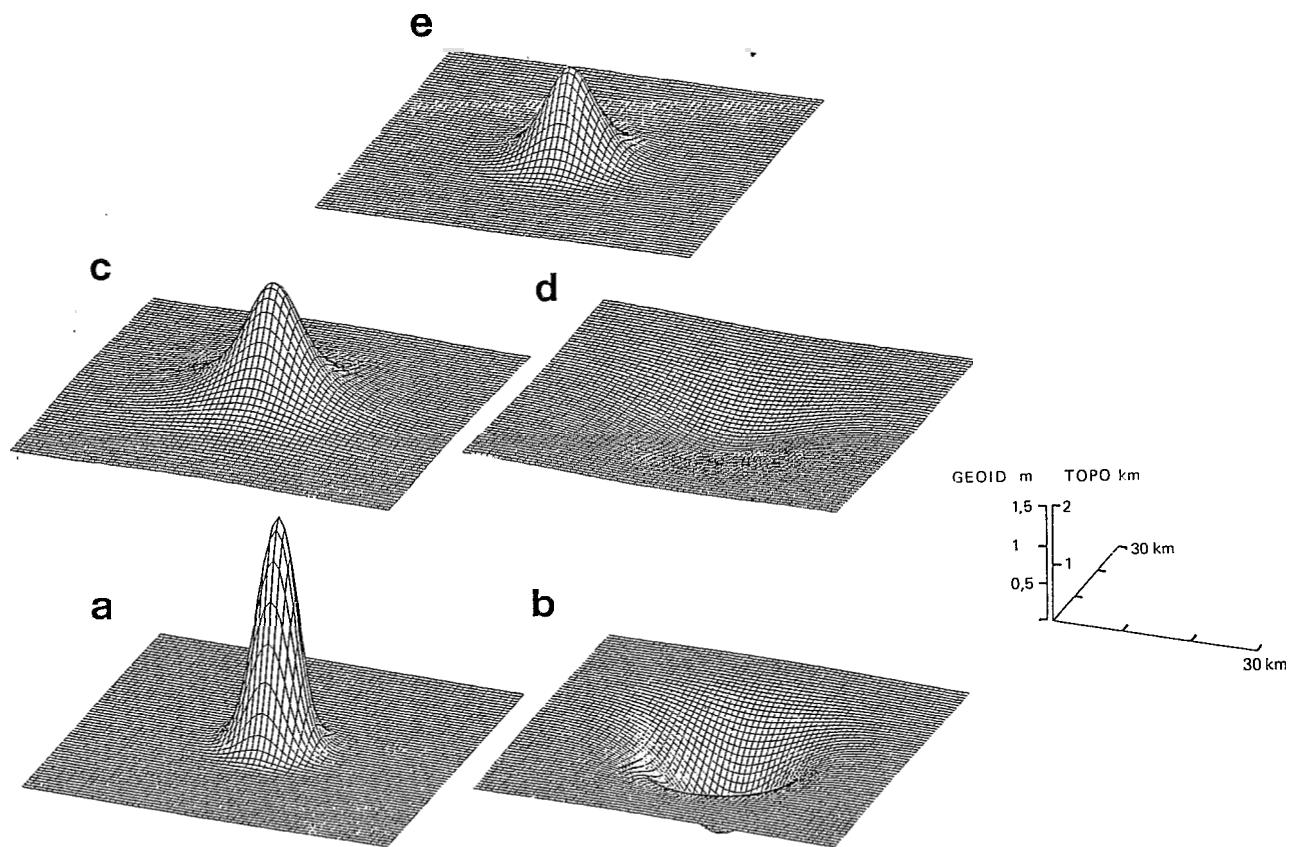
Figure 3. Gaussian seamount lying over a 5 km thick elastic lithosphere and corresponding geoid. (a) Topography of the Seamount. (b) Geometry of the deflected Moho. (c) Geoid anomaly due to the seamount topography only. (d) Geoid anomaly due to the deflected Moho. (e) Total geoid anomaly due to the excess topography and its isostatic support.

In order to model the geoid signature we must take into account

— the shape of the seamount
— its density and the crustal density
— the depth of the Moho discontinuity
— the geometry of the Moho discontinuity
— the distance of the seamount to the altimetric track.

Now we discuss these parameters.

It has been shown (Lacey, Ockendon & Turcotte 1981; Angevine & Turcotte 1984) that in a given geographic area all seamounts have approximately the same mean slope independent of their height and that their shape is well represented by a Gaussian function (Watts & Ribe 1984). Thus, the parameter which best defines the shape of the seamount is its height.
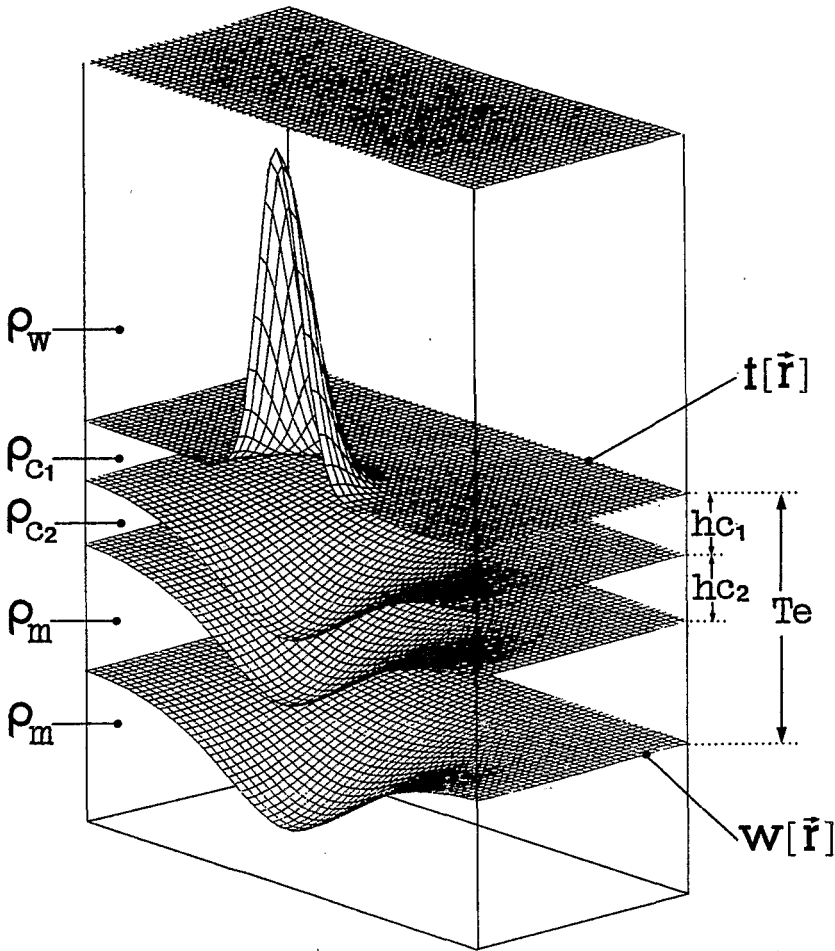

Figure 4. Crustal model used in this study. $t(r)$ and $w(r)$ are, respectively, the topographic surfaces and the surface which models the deflected interfaces. hc1 and hc2 are the crustal thicknesses and Te is the effective elastic thickness. ρ_W, ρ_{C_1}, ρ_{C_2} and ρ_m are water, crustal and mantle densities. The interface shown at the bottom of the elastic layer has no physical significance.

Densities vary from about 2.4 for the upper part of the crust to 3.4 for the upper mantle. A mean density of 2.8 for the load and the crust is commonly used in the case of a one-layered crust. But, as shown by Lambeck (1981), such a value for the load might be an over-estimate and a slightly smaller value (2.5, for example) is more appropriate. In the present study we use a two layered crust (Fig. 4) based on results obtained from seismic refraction carried out in the northern part of the Cook archipelago (Woollard 1975). The upper part is 2.5 km thick and has a density ρ_{c1} of 2.5 and the lower part is 5 km thick with a density ρ_{c2} of 2.9. The density of the upper mantle ρ_m is taken as 3.35.

The crustal thickness is also fixed using results of refraction data. Nevertheless, it must be noted that a variation of the crustal thickness yields a variation in the geoid anomaly.

The analysis of flexure of the lithosphere under loads has been carried out in many areas and a simple model has been shown to satisfactorily explain the data (Dubois, Launay & Recy 1974; Watts & Cochran 1974; Watts, Cochran & Seltzer 1975; Cazenave *et al.* 1980). In this model, the lithosphere is treated as a continuous layer behaving elastically. Thus, the deformation for a given load is controlled by a single parameter: the elastic thickness. The model of a continuous plate is, of course, an approximation. For example, recent multi-channel seismic results (Watts *et al.* 1985b) have shown that the lithosphere beneath the Hawaiian chain is probably fractured as it has been postulated earlier by Walcott (1970). In that case the elastic thickness must be analysed in terms of an equivalent (or effective) elastic thickness of a continuous plate which models the mechanical behaviour of the litho-sphere. The effective elastic thickness (EET) is related to the age of the lithosphere (Watts 1978). Combining a wide range of results, Bodine, Steckler & Watts (1981) have shown that the EET is related to the square root of the age of the lithosphere at the time of loading. In other words, the EET corresponds to the depth at a given isotherm.

Nevertheless, as pointed out by McNutt (1984), deviations from this law might occur due to some complications in the emplacement process. McNutt demonstrated that if the emplacement of a seamount chain is associated with a large thermal event, some thermal rejuvenation will take place. Then the elastic thickness which will control the deformation of the plate will be smaller than the one deduced from the above-mentioned law. Therefore, she proposed to use a thermal age deduced from the bathymetry rather than a crustal age deduced from magnetic anomalies when considering loads superimposed on a broad bathy-metric swell. For example, in the case of Hawaii, her results or those of Ten Brink & Watts (1985) demonstrate that the elastic thickness corresponds better to an age younger than the $\simeq$ 80 Myr for the lithosphere at the time of loading.

So, following Watts & Ribe (1984), it appears that two classes of seamounts must be considered. Some seamounts are created near the ridge crest by some abnormal regime of the ridge system as, for example, the Ob, Lena and Marion Dufresne seamounts in the Southwest Indian Ocean (Diament & Goslin 1986). Other seamounts are created on an old plate by some intraplate volcanism, e.g. most of the Pacific seamounts such as the Hawaiian chain. The first type, called on-ridge seamounts, are associated with a low elastic thickness, typically less than or about 5 km. The second type, off-ridge seamounts, are associated with a larger elastic thickness ranging from about 10 km to 35 km.

Fig. 5 displays the results of some computations concerning the effects of these various parameters. The geoid anomalies are computed over a Gaussian seamount of 3 km height. Fig. 5(a) shows that the amplitude of the computed anomaly increases by about 15 per cent with an increase of 0.2 g cm^{-3} of the load density and that the wavelength is independent of the elastic thickness Te. In this computation the crust is taken as a single layer with a thickness of 7.5 km. Fig. 5(b) shows the effect of the variation of the crustal thickness. As expected, the discrepancies are larger for a smaller value of Te than for a larger value.
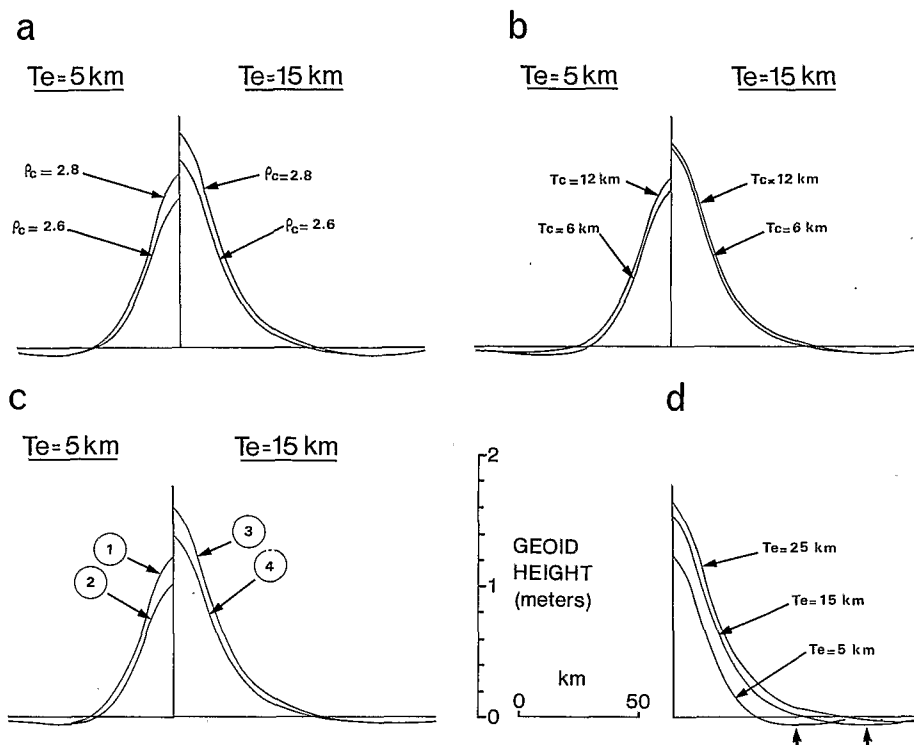
a

Te = 5 km   Te = 15 km

$\rho_c = 2.8$ $\rho_c = 2.8$

$\rho_c = 2.6$ $\rho_c = 2.6$

b

Te = 5 km   Te = 15 km

Tc = 12 km   Tc × 12 km

Tc = 6 km   Tc = 6 km

c

Te = 5 km   Te = 15 km

1   3
2   4

d

2

GEOID
HEIGHT
(meters)

1

km

0   50

0

Te = 25 km

Te = 15 km

Te = 5 km

Figure 5. Influence of variation of various model parameters. The geoid anomaly is computed for a Gaussian seamount of 3 km high. (a) Variation of the crustal and load density from 2.6 to 2.8. The crust is assumed to be an unique layer of 7.5 km thick. Densities of sea water and mantle are taken as 1.03 and 3.4, respectively. Two elastic thicknesses, corresponding to an off-ridge and an on-ridge emplacement, are taken into account. (b) Variation of the crustal thickness from 6 to 12 km. The crust is assumed to be a unique layer with a density of 2.7. (c) Comparison between the geoid anomalies computed for the seamount lying over a single layered crust of 7.5 km thick with a density of 2.7 (curves 1 and 3) and over a two layered crust with an upper part 2.5 km thick with a density of 2.5 and a lower part 5 km thick with a density of 2.9 (curves 2 and 4). (d) Influence of the effective elastic thickness. Computations have been made with a single layered crust of 7.5 km thick and with a density of 2.7. The E.E.T. is the only parameter which has effects both on amplitude and on the wavelength of the seamount signature.

Nevertheless these variations appear to be small. A comparison between a single layer crust and a multilayered one is shown on Fig. 5(c). Comparison of results shown in Fig. 5(c) with those shown in Figs 5(a) and (b) demonstrates that the controlling parameter of the crustal model is the density of the upper part of the crust and of the load. The influence of density is much larger than those of crustal thickness or of layer structure of the crust. It should be noted that variation of the density structure produces changes in the amplitude, and not in the wavelength, of the anomaly. Fig. 5(d) shows variation of the geoid anomaly for various Te. The response of the geoid anomaly is very different for Te than it was for density. The discrepancies in the computed geoid are large between the on-ridge and the off-ridge classes but fortunately not very large within the off-ridge class. This is shown most clearly on the minimum of the curves as indicated by the two arrows on Fig. 5(d).

To precisely locate a seamount we need two tracks. Otherwise, there are two possible locations, one on each side of the altimetric profile. With more than one profile, the seamount is located in a direction going through the maximum of the observed anomalies and

normal to the parallel SEASAT tracks. Of course, the seamount will be closer to the track which presents the larger anomaly and there will be only one possible location.

Method of location

We seek the best least-square fit between observed and theoretical geoid anomalies over a possible seamount visually detected on SEASAT profiles. The observed anomalies are assumed in most cases to be detected on at least two neighbouring sub-satellite altimetric tracks. The theoretical anomalies along profiles are extracted from a computed theoretical map since the geoidal signature of a seamount is typically 3-D (Fig. 3). Maps are computed for various parameters. The deformed crustal interface $w(x, y)$ is simply related to the bathymetric surface $b(x, y)$ in the Fourier domain (Banks, Parker & Huestis 1977) by

$$W(\mathbf{k}) = \frac{-g(\rho_{c1} - \rho_w)\, B(\mathbf{k})}{D|\mathbf{k}|^4 + g(\rho_m - \rho_{c1})},$$

where $\mathbf{k}$ is the wavenumber vector, and D, the flexural rigidity, is simply related to the elastic thickness Te by,

$$D = \frac{E\, \mathrm{Te}^3}{12(1 - \nu^2)}$$

with E the Young modulus and ν the Poisson's ratio. ρ_w, ρ_{c1} and ρ_{c2} are, respectively, the density of the water (1.03), of the upper crust and of the load (2.50) and of the mantle (3.35) and g is the gravitational acceleration, $9.81~\mathrm{m~s^{-2}}$.

The gravity anomaly due to any interface $h(x, y)$ lying at a depth below sealevel z and with a density contrast ρ is (Parker 1972) in the wavenumber domain

$$G(\mathbf{k}) = 2\pi\rho\, \mathscr{G} \exp\left(-|\mathbf{k}|z\right) \sum_{n=1}^{n=\infty} \frac{|\mathbf{k}|^{n-1}}{n!}\, \mathrm{FT}\left[h^n(x, y)\right].$$

FT denotes the Fourier transform and $\mathscr{G}$ is the acceleration constant.

The geoid anomaly $H(\mathbf{k})$ in the wavenumber domain is deduced from the gravity anomaly using the relation (Chapman 1979)

$$H(\mathbf{k}) = \frac{G(\mathbf{k})}{g|\mathbf{k}|}$$

$$H(\mathbf{k}) = \frac{2\pi\rho\mathscr{G}}{g} \exp\left(-|\mathbf{k}|z\right) \sum_{n=1}^{n=\infty} \frac{|\mathbf{k}|^{n-2}}{n!}\, \mathrm{FT}\left[h^n(x, y)\right].$$

We only retained the first two terms of the sum since higher terms did not appear to be significant.

The geoid anomalies are computed for all the interfaces involved using a 2-D fast Fourier transform algorithm and then summed. The resulting anomaly is then converted back into the space domain using an inverse Fourier transform. Since we deal with synthetic topographic surfaces with edges which are gently set to zero (Fig. 3), no specific treatments have been applied to the data in order to avoid possible aliasing due to an edge effect (Diament 1985). It can be noted that since the problem has cylindrical symmetry, Hankel transform could have been used instead of the 2-D Fourier transform. We chose the Fourier transform for computing facility.

After inspection of published data and maps in the Austral area (Summerhayes 1967; Mammerickx *et al.* 1975; Johnson 1980) we chose a mean slope of 4.6° for the model of a seamount. We fixed the crustal model from the above mentioned results of refraction data. Therefore, the only parameters that we consider are the distance d between the seamount and the closest profile, the height of the seamount h and the effective elastic thickness Te. From the results shown previously we consider the possible deviation in the seamount density and in the crustal thickness included within Te. In other words, the effective elastic-thickness that we consider may differ from the elastic thickness of the lithosphere beneath the seamount if other values of ρ_c and Tc are considered. This approximation is valid only because our goal is primarily to locate uncharted seamounts and to give an estimation of their size and not to precisely determine Te.

Synthetic profiles have been computed for a wide range for d, h and Te values: d varying from 0 to 100 km with a step of 1 km; h varying from 0.2 to 4.5 km with a step of 0.1 km; Te varying from 5 to 30 km with a step of 5 km.

Test with synthetic data

In order to check our method we first extracted theoretical anomalies along profiles from the 3-D anomaly computed for a given seamount and then relocated the seamount. Computations have been made for various heights of seamounts, elastic thicknesses and distances between the axis of the seamount and the tracks.

Fig. 6 shows the results of such a computation for a 4 km high seamount and with two profiles (track 1 and 2) lying 15 km and 25 km, respectively, from the seamount axis (Fig. 6a). The theoretical geoid anomaly along the two tracks was first computed assuming an off-ridge seamount (Te = 15 km). We then relocated the seamount using the two computed synthetic geoid anomaly profiles and assuming various heights, locations and elastic thicknesses. Fig. 6(b) shows the resulting topography for three assumed elastic thicknesses, each topographic profile corresponding to the best RMS fit obtained using both geoid anomaly profiles. The right location and height is, of course, obtained when the elastic thickness used for the relocation is equal to the assumed one (Te = 15 km). Fig. 6(c) shows the results of identical computations except that there the seamount has been assumed on-ridge (Te = 5 km). It appears in both cases that the position of the axis of the seamount is within 10 km of the input one. Fig. 7 shows contours of the RMS error plotted as a function of the height and of the distance to the closest altimetric profile for various Te. Figs 7(a) and (b) correspond to the location of an off-ridge (Te = 15 km) and an on-ridge (Te = 5 km) seamount respectively. When the chosen elastic thickness is that of the forward model, the minimum of the RMS error is zero. The value of the minimum RMS error increases when the deviation between the real Te and the assumed one increases. Since the error on the amplitude of the geoid anomalies as given by SEASAT is 8 cm (Lame & Born 1982) we assume that the error on our computation is given by the contour on these plots corresponding to a deviation of 8 cm from the minimum. For example, the worst case is obtained assuming Te = 30 km for an on-ridge seamount. In this case the lateral mislocation is about 25 km (Fig. 7b). When the correct Te is assumed for the computation, the lateral error is less than 10 km. Similar results were obtained for the other studied cases. Therefore, we conclude that for noiseless synthetic data the lateral error of the location of the sea-mount is less than 15 km when the elastic thickness is known fairly well. These results also confirm that inside the off-ridge class, knowledge of the exact elastic thickness is not necessary to precisely locate the seamounts. The computed height may be in error by 50 per cent if the elastic thickness is significantly overestimated; the error is slightly less if the
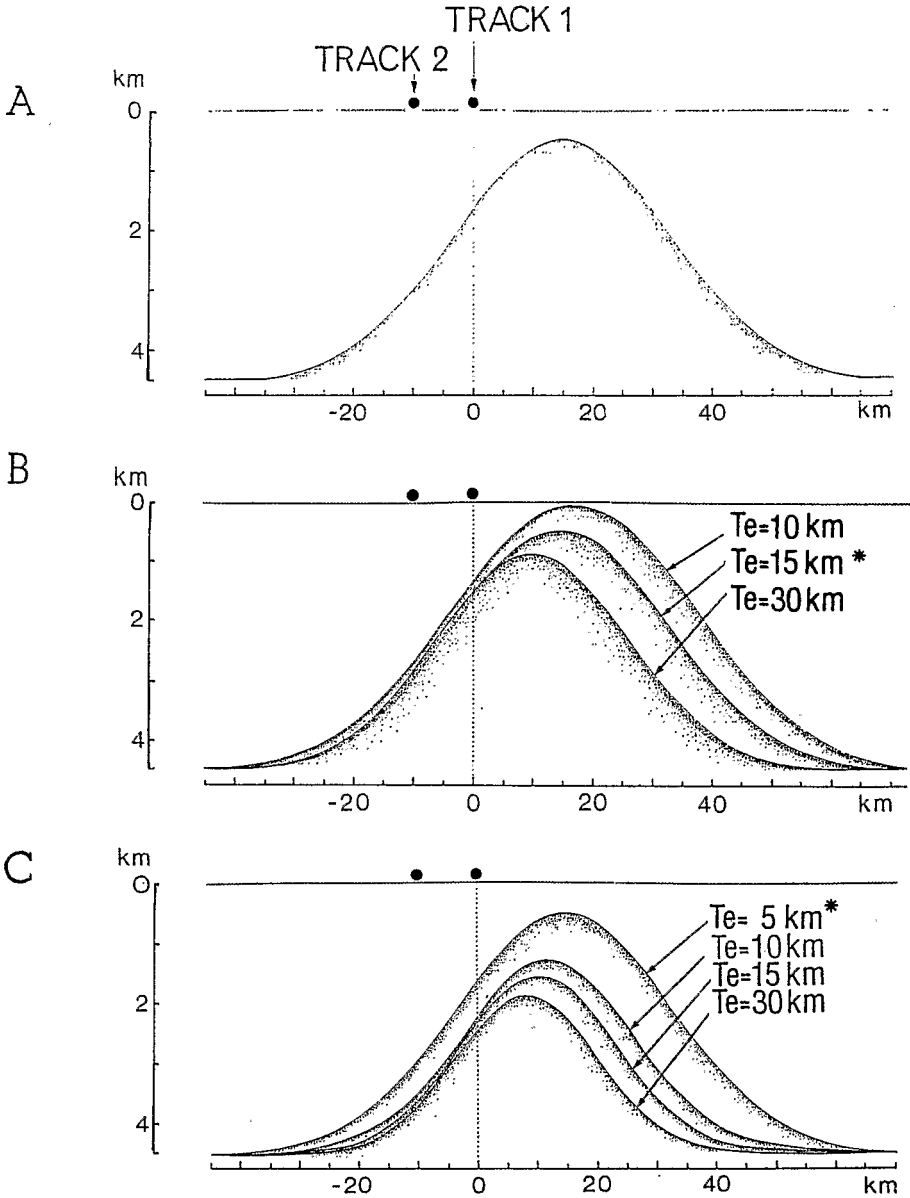
Figure 6. Location of a 4 km high synthetic seamount detected on two profiles lying 15 km and 25 km, respectively, off-axis from the centre of the seamount. (a) Synthetic topography. (b) Recomputed topography as a function of various elastic thicknesses. The synthetic seamount was assumed to be over a 15 km thick elastic thickness. (c) Same as figure b, but the synthetic seamount is assumed to be on 5 km thick elastic thickness.

elastic thickness is significantly underestimated. In most cases, the precision is about 20 per cent. If the anomaly is detected on only one profile, the determination of the distance to the profile is much worse, with location errors of about 50 km. Furthermore, as noted previously for anomalies detected on only one profile, we do not know on which side of the profile the seamount is located. Thus, it is impossible to precisely locate a seamount
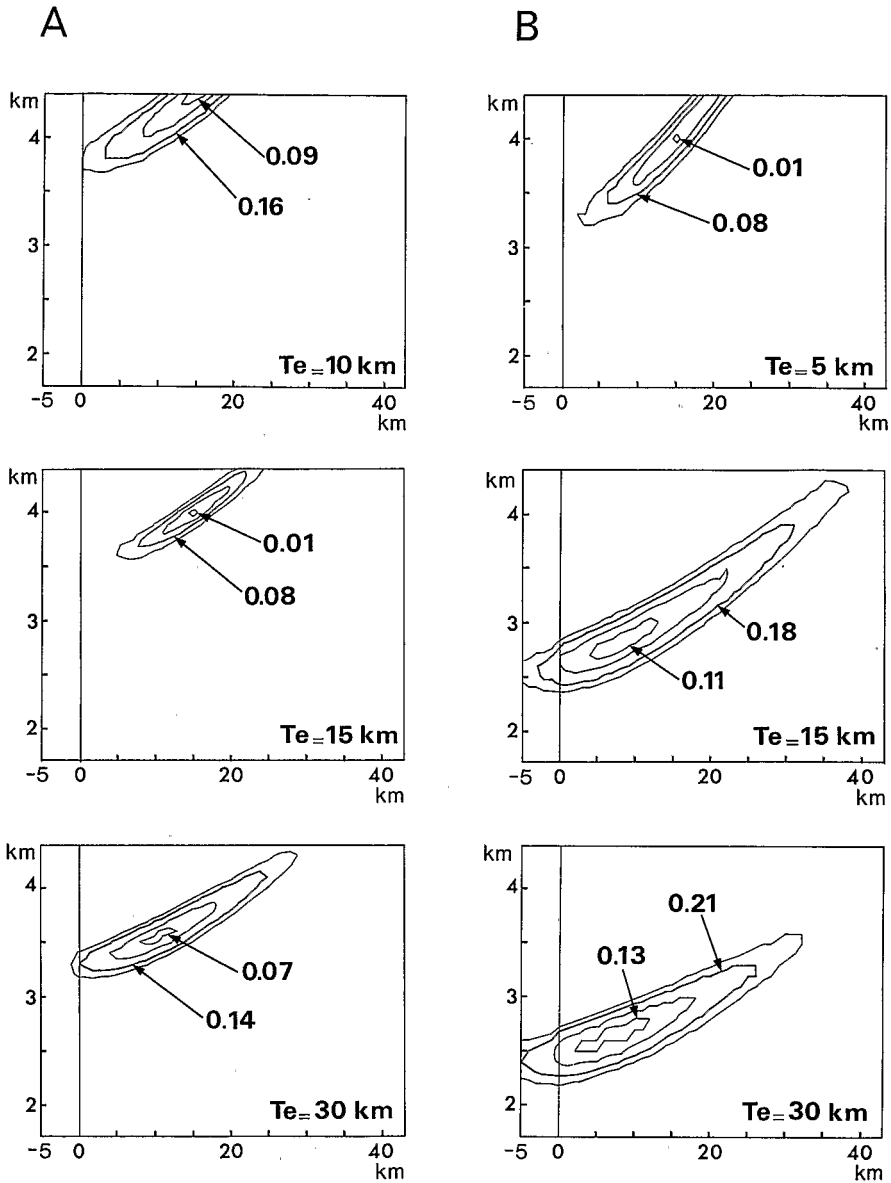
A

B

Figure 7. Plot of the RMS error in meters for the synthetic data shown in Fig. 6. Each graph shows four contours corresponding to the minimum RMS value plus 1 cm, 4 cm, 8 cm and 12 cm, respectively. Horizontal axis corresponds to the distance of the seamount to the closest satellite track and the vertical axis to the height of the seamount.

detected on one profile even when taking into account parameters such as the elastic thickness.

The Austral archipelago

Fig. 1 displays the SEASAT tracks superimposed on the main bathymetric features taken from the GEBCO charts. Two main directions for alignments bathymetry observed in the

South Central Pacific are: the present N110°E orientation of spreading at the East Pacific Rise; and the N70°E associated with the pre ridge-jump Farallon regime. In the present study area, the Austral volcanic chain has a N110°E azimuth while the Austral Fracture Zone, which intersects the chain approximately between the islands of Raivavae and of Tubuai, is oriented N70°E. The age of the lithosphere in the area as given by either magnetic anomalies or a map of isochrons (Herron 1972; Sclater, Jaupart & Galson 1980) lies approxi-
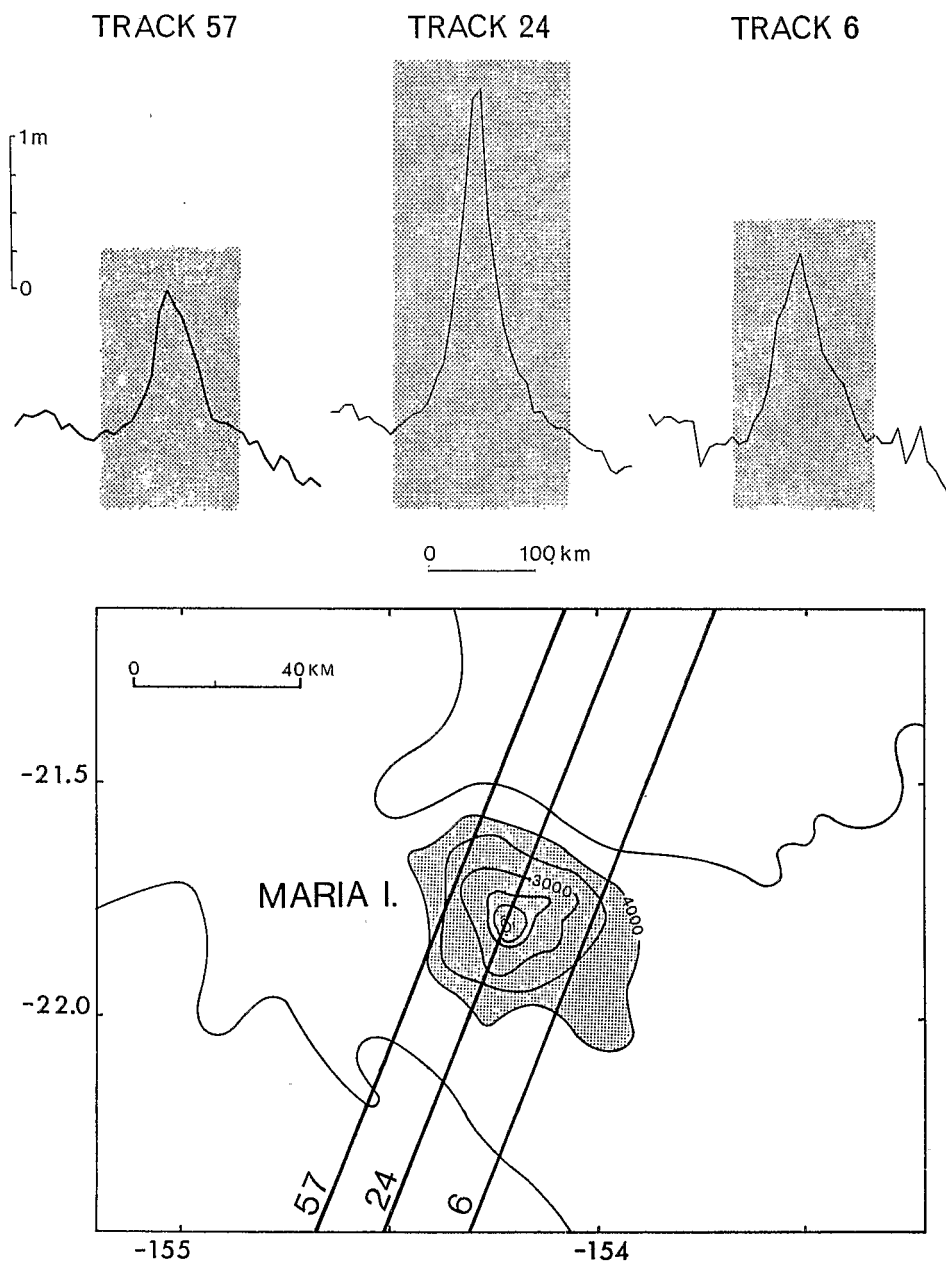
TRACK 57   TRACK 24   TRACK 6

Figure 8. Location and observed SEASAT tracks over the Maria Island. Dashed area on the profiles corresponds to the anomaly used for the location.
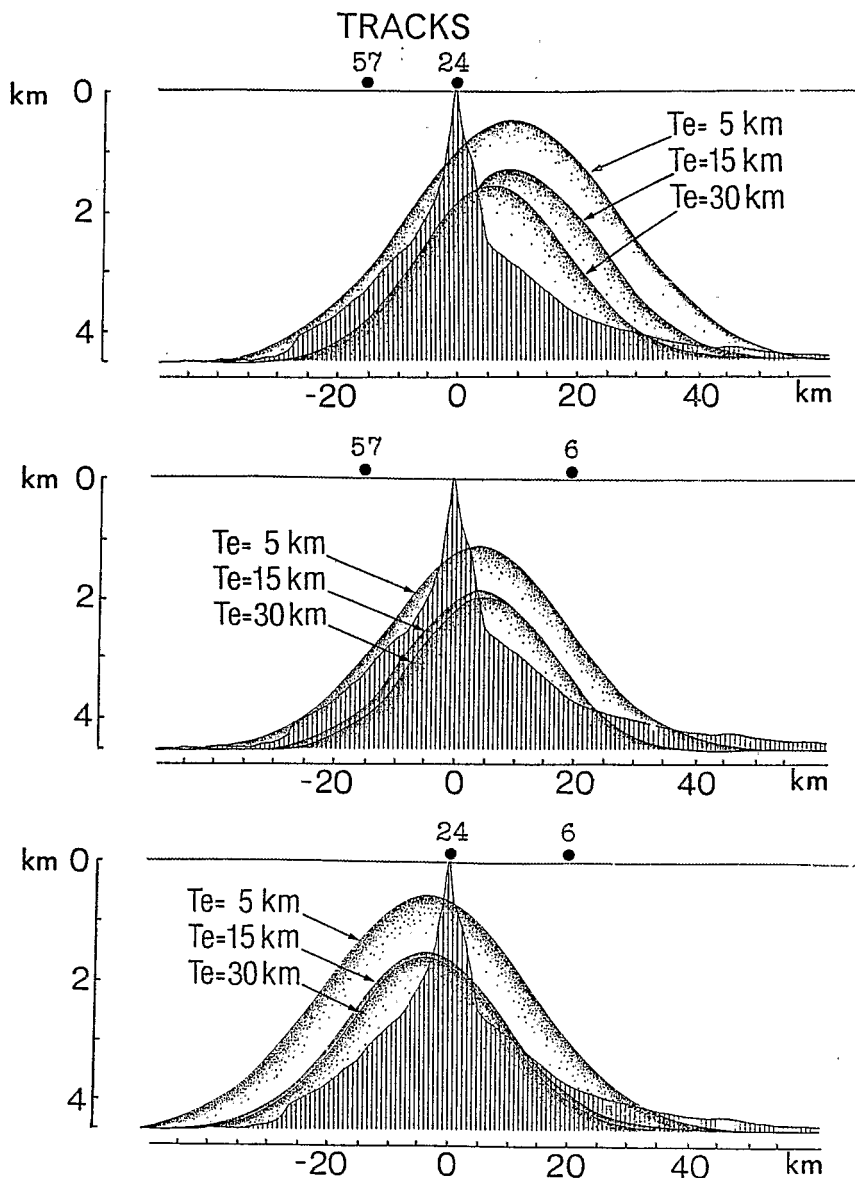
Figure 9. Result of the relocation of Maria Island using the various pairs of SEASAT profiles. The area with stripes is the actual island as taken from the Mammerickx charts. The computed position is within 10 km of the position of the island and the Gaussian shape fits the volcanic basement if an off-ridge origin is assumed.

mately between 40 Ma and 70 Ma. Potassium–Argon dates have also been published for some of the islands (Jarrard & Clague 1977; McDougall & Duncan 1980). It clearly appears that these islands have been emplaced on an old lithosphere and therefore that the structures in the area must (*a priori*) be considered off-ridge.

Three SEASAT tracks run close to the Maria Island (Figs 1 and 8). This island consists of a coral reef built over a submarine volcano. We relocated this island using the three couples of profiles available. Results are shown on Fig. 9. The area with stripes represents the island
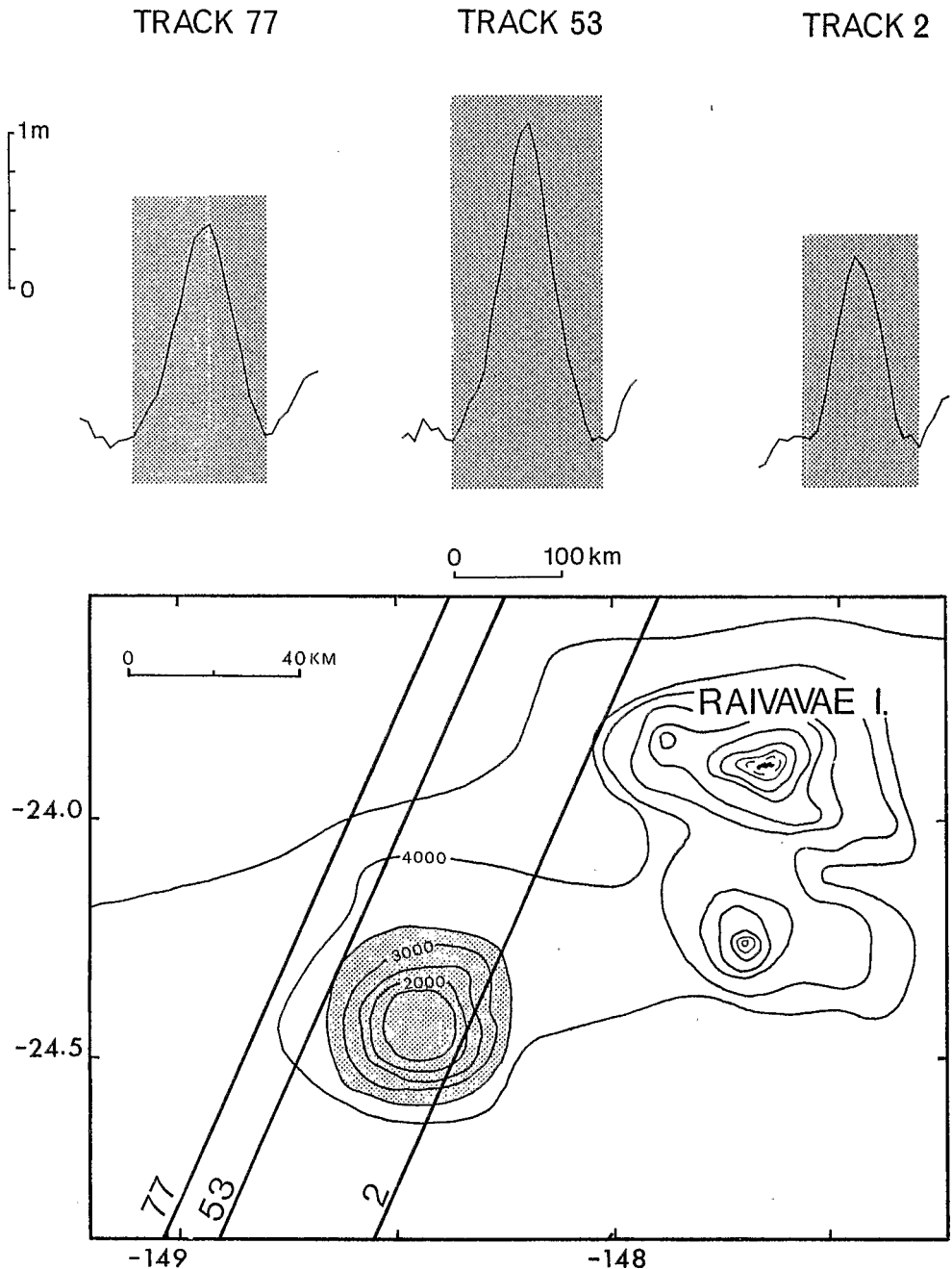
TRACK 77   TRACK 53   TRACK 2

Figure 10. Location and observed SEASAT tracks over an unnamed seamount southwest of Raivavae.

as located on the Mammerickx map and the curves correspond to the best computed shape and location according to the RMS error values for various Te. The Gaussian shape of the theoretical seamount fits well the shape of the volcanic basement of the island but of course cannot take into account the reef. The discrepancy between the computed location and the charted one is less than 10 km, thus confirming with real SEASAT data the results obtained
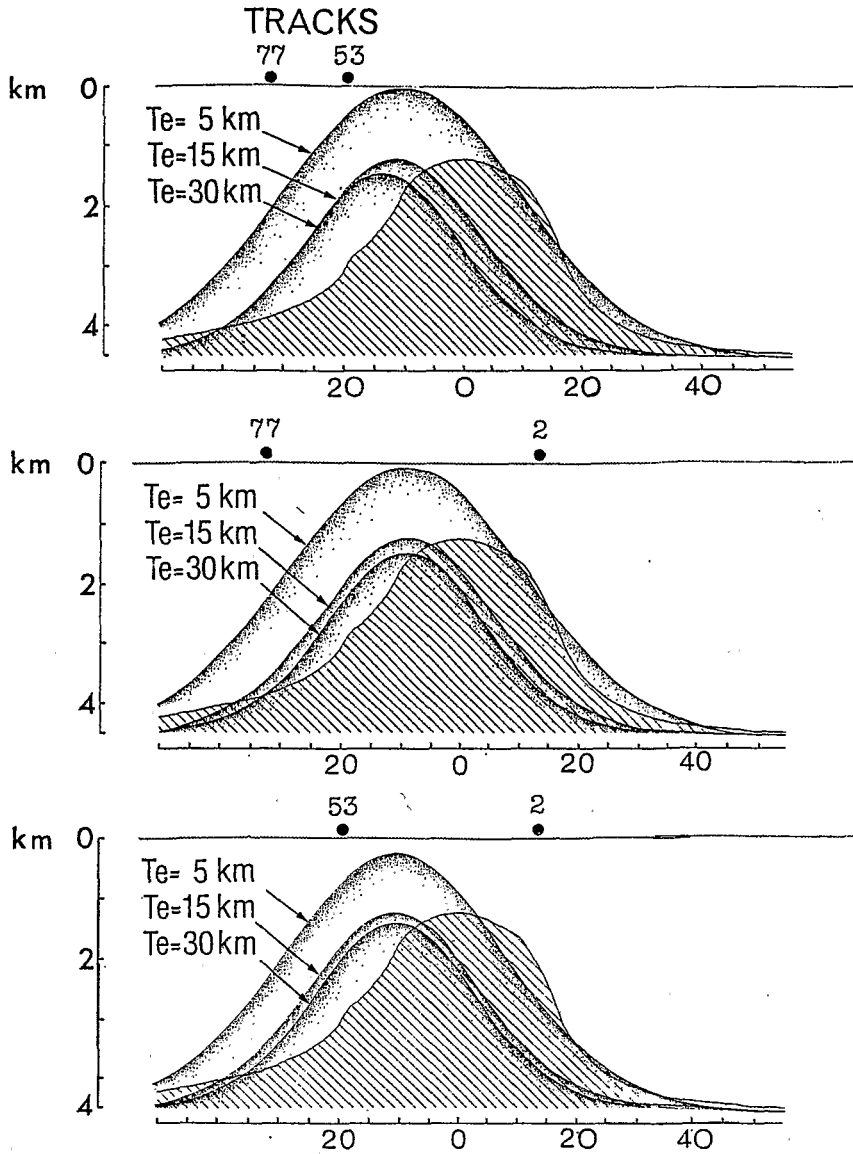
TRACKS

Figure 11. Results of the relocation of the unnamed seamount for various pairs of SEASAT data. The area with stripes represents the seamount as given by chart. The theoretical Gaussian seamount fits the real one very well if an off-ridge origin is assumed. A systematic shift to the west is obtained and is probably due to an error in the published chart.

with synthetic profiles. Our method predicts a reasonable height of the volcanic basement since the Maria atoll is built on an off-ridge volcano as indicated before. The minimum value of the RMS error is about 15 cm. What does the minimum RMS value computed with SEASAT data mean? If the assumed seamount morphology, crustal model and lithospheric elastic thickness are very close to the real ones, then the computed RMS should be close to a minimum value. This minimum value differs from zero since the SEASAT data are noisy due to e.g. orbital errors, oceanographical residual effects or instrumental noise (Brammer &

Table 1. Location and size of the detected seamounts in the Austral area. The precision of the location is within 15 km, except for S1 and S4 which were detected on only one SEASAT track.

	Number of tracks	Minimum RMS meters	Location Lat.	Long.	Size $T_e = 30$ km meters
S1	1	0.10	−20.53	−156.93	3000
S2	2	0.03	−20.96	−152.32	2000
S3	2	0.12	−21.49	−155.52	2100
S4	1	0.12	−22.89	−154.74	1700
S5	3	0.08	−23.71	−154.28	1700
S6	2	0.15	−24.13	−156.41	2600
S7	2	0.08	−25.20	−153.15	1500
S8	2	0.10	−25.57	−150.48	2400
S9	2	0.18	−25.60	−150.07	3100
S10	2	0.16	−27.35	−145.26	3200

Sailor 1980). In order to estimate this minimum value, we analysed residual profiles obtained by subtracting from each other repeat SEASAT tracks over some known seamounts in the Austral Islands archipelago. The RMS values were computed using the same approach as the one used for locating seamounts and it appears that these values are of the order of 3–4 cm. The minimum RMS value obtained for Maria can thus be explained by the discrepancy between the real and assumed morphology.

The second test with real data deals with a seamount charted approximately 100 km southwest of the Raivavae island (Figs 1 and 10). Results are shown on Fig. 11. It appears
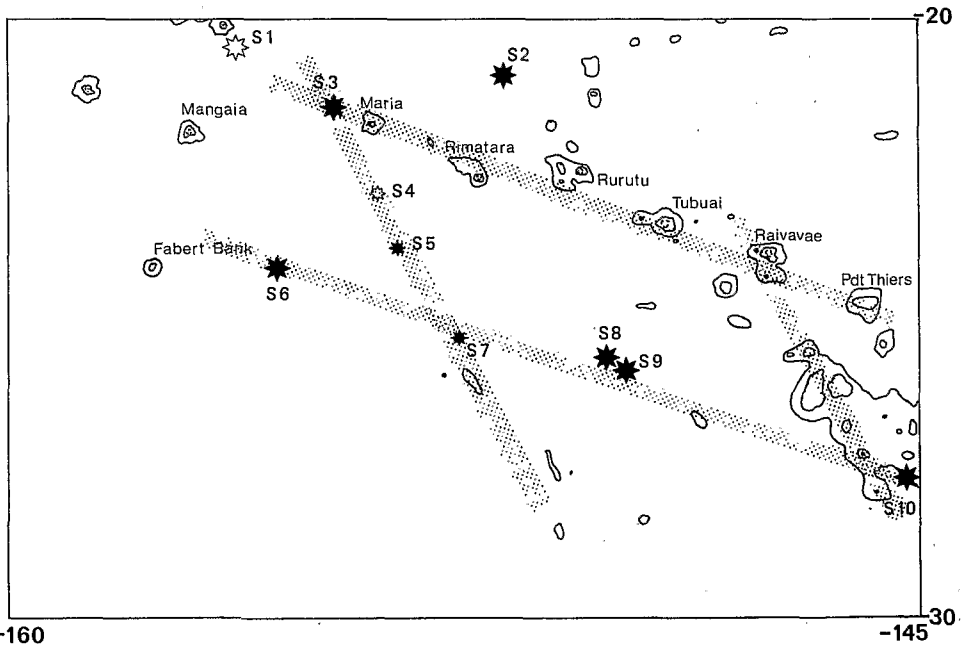

Figure 12. Location of the ten detected seamounts in the Austral archipelago. Two of them (S4 and S1) have been detected on only one profile (see text). S6, S7, S8, S9 and S10 lie along the extension of the southern chain of the archipelago. S3, S4, S5, S7, lie along the northward extension of some charted bathymetric features and a lineament that is detectable on published maps of geoid.

that the charted shape and height of this seamount are very well modelled when an off-ridge origin is assumed. The minimum RMS error is less than 12 cm, smaller than the one obtained for Maria atoll. Nevertheless, this value is still larger than the one which could be expected for such a fit between the computed morphology and the charted one. Examination of the GEBCO and Mammerickx charts show that no cruise passed over this seamount and that therefore, its charted morphology is probably deduced from limited bathymetric sounding. A systematic shift to the northeast of about 13 km is obtained with the three couples of SEASAT profiles used. This is logical, since the largest anomaly is observed on the track 53 (Fig. 10) and not on the track 2 which is located closer to the top of the charted seamount. Thus we believe that the shift is real and therefore that this seamount is mischarted on both GEBCO and Mammerickx charts. Such a mispositioning is not surprising with bathymetric features located using pre-satellite marine positioning. This result also confirms the reliability of the location of seamounts from SEASAT data. It also appears that the heights computed assuming an off-ridge emplacement are very reasonable as long as no coral reef is present. The value of the minimum RMS error is an indication of the quality of the fit. The smaller the RMS error, the closer is the shape of the uncharted seamount to our Gaussian model. Moreover these results confirm that our choice of varying Te while fixing the crustal density and thickness structure is adequate. We next turn to the results of interpretation of SEASAT data in the studied area.

Ten previously uncharted seamounts have been detected in the area. Locations and heights are given in Table 1 and in Fig. 12. We assumed that all these seamounts were emplaced off-ridge, and the location is given with a lateral precision of 15 km. Two of them, S1 and S4, were detected on only one SEASAT profile so the position given corresponds to the maximum of the anomaly on the SEASAT track. One can notice that a descending GEOS-3 profile runs close to S1. Although the GEOS-3 profiles are noisy and less accurate than SEASAT data, the along-track deflection of the vertical suggests that S1 is exactly located slightly to the southwest (Sandwell 1984b). The existence of four seamounts (S1, S3, S5, S6) has been mentioned previously by Lambeck & Coleman (1982) who did not precisely locate them. We also confirm the major mispositioning of Fabert Bank on both Mammerick and GEBCO chart mentioned by Lambeck & Coleman. There is no geoid anomaly over this important feature. Even if this postulated seamount was emplaced on-ridge and was fully compensated, there should be a detectable signature on the track running immediately above it. Therefore we assume that Fabert Bank is the detected seamount S6, and that the mispositioning is of about 200 km to the west.

Discussion of these results

In a recent study, Calmant & Cazenave (1986) inspected the effective elastic thickness beneath all the known islands and seamounts of the Austral chain using SYNBAPS bathymetric data and SEASAT geoid data. They found that the range of the EET of the lithosphere lies between 4 km for MacDonald volcano and 10 ± 1 km for Maria island. Our larger values of Te for Maria and for the unnamed seamount southwest of Raivavae may be considered consistent with their thickness since they used a density of 2.8 for the entire topographic load. But the elastic thickness deduced from the age of the lithosphere at the time of loading (e.g. Bodine *et al.* 1981) in this area appears to be much larger than these values. Such an abnormally low EET seems to be specific for the Cook—Austral chain, e.g. the Society Islands do not have low EET values (Calmant & Cazenave 1986). This is an indication of abnormal behaviour from the postulated hotspot.

The seamounts located in the present study appear on well-defined azimuths (Fig. 12).

21

Five of them, S6, S7, S8, S9 and S10, respectively, are located along the extension of the postulated southern chain. Thus we confirm the existence of two parallel and distinct chains oriented N110°E. Seamounts S3, S4, S5 and S7 (respectively) are aligned in a N150°E direction along the extension of some bathymetric features in the south. A close examination of the illumination map of Sandwell (1984a) or of the geotectonic image of Haxby (Francheteau 1983) confirms the existence of this lineament oriented N150°E. It is tempting to assume that this direction is also present in the eastern part of the studied area: some seamounts are located on a line N150°E going through Raivavae (Fig. 12). Thus, the seamounts and islands in the Austral zone appear to be located in directions which intersect each other. A possible explanation would be that the volcanic features of the Austral archipelago have been emplaced by the action of various hotspots. One can also notice that these lineaments form a rhombus with a more developed northern side. This kind of geometrical form is also observed in continental volcanic areas such as the Nigerian alkaline Younger Granites province in Africa (Lameyre *et al.* 1984; Black, Lameyre & Bonin 1985). Such a distribution of volcanic structures cannot be easily reconciled with a concept of a single hotspot cutting the lithosphere when it passes above it in a very narrow stripe. Therefore, we propose that the seamounts and islands of the Austral archipelago are the superficial expression of a broad thermal event whose origin has yet to be examined (Diament & Baudry, in preparation). This assumption is supported by the geographical distribution of the seamounts, by the abnormally thin effective elastic-thickness and by the existence of a large bathymetric swell in the Cook—Austral area.

Summary and conclusion

(1) The ability to detect the existence of uncharted seamounts using SEASAT data has been confirmed. The precision of the location is up to about 15 km if the anomaly is detected on at least two SEASAT tracks and if the tectonic setting of the seamount is reasonably well known. An estimate of the size may also be obtained with good confidence.

(2) Examination of SEASAT data in the western part of the Austral archipelago, south central Pacific, reveals the existence of some mispositioning in published charts and of ten uncharted seamounts.

(3) The spatial distribution of all the topographic features in the Austral archipelago, combined with previously published results, leads us to postulate that this archipelago is emplaced over a broad, abnormal thermal event.

A confirmation of these results was recently obtained in January 1986 during the SEAPSO (Leg V) cruise of the N/O Jean-Charcot — see Pontoise *et al.* (1986) for the preliminary results. A complete interpretation of the data gathered on this cruise is in preparation (Baudry & Diament, in preparation). The charted location of Fabert Bank and the locations of the seamounts S2, S5 and S6 given here were surveyed using SEABEAM equipment. No topographic feature was present in the area of the charted Fabert Bank and three seamounts were found in the predicted locations. Moreover, it appeared that the shape of S2 is more regular than the shape of S5 while S6 presents two summits. This favours our interpretation of the RMS values.

References

Angevine, C. L. & Turcotte, D. L., 1984. Geometrical form of aseismic ridges, volcanoes and seamounts, *J. geophys. Res.,* **89,** 11 287–11 292.

Banks, R. J., Parker, R. L. & Huestis, S. P., 1977. Isostatic compensation on a continental scale: local versus regional mechanisms, *Geophys. J. R. astr. Soc.,* **51,** 431–452.

Barsczus, H. G., 1980. *Les Îles Australes (Polynésie Française) et la théorie des points chauds. Notes et Doc. (Géophys.)* Centre ORSTOM de Papeete, no. 1980/27.

Barsczus, H. G. & Liotard, J. M., 1985. Contribution à la connaissance pétrographique et géochimique de l'île de Rawavae (Polynésie Française, Océan Pacifique Centre Sud), *C. r. Acad. Sci., Paris,* **301 (20),** 1409–1412.

Black, R., Lameyre, J. & Bonin, B., 1985. The structural setting of alkaline complexes, *J. African Earth Sci.,* **3,** 5–16.

Bodine, J. H., Steckler, M. S. & Watts, A. B., 1981. Observations of flexure and the rheology of the oceanic lithosphere, *J. geophys. Res.,* **86,** 3695–3707.

Brammer, R. F. & Sailor, R. V., 1980. Preliminary estimates of the resolution capability of the SEASAT Radar Altimeter, *Geophys. Res. Lett.,* **7,** 193–196.

Calmant, S. & Cazenave, A., 1986. The effective elastic lithosphere under the Cook-Austral and Society islands, *Earth planet. Sci. Lett.,* **77,** 187–202.

Cazenave, A., Lago, B., Dominh, K. & Lambeck, 1980. On the response of the ocean lithosphere to seamount loads from Geos 3 satellite radar altimeter observations, *Geophys. J. R. astr. Soc.,* **63,** 233–252.

Chapman, M. E., 1979. Techniques for interpretation of geoid anomalies, *J. geophys. Res.,* **86,** 3793–3801.

Diament, M., 1985. Influence of data analysis on admittance computation, *Annales Geophysicae,* **3(6),** 785–792.

Diament, M. & Goslin, J., 1986. Emplacement of the Marion Dufresne, Lena and Ob seamounts (South Indian Ocean) from a study of isostasy, *Tectonophys.,* **121,** 253–262.

Dixon, T. H. & Parke, M. E., 1983. Bathymetry estimates in the southern ocean from SEASAT altimetry, *Nature,* **304,** 406–411.

Dubois, J., Launay, J. & Recy, J., 1974. Uplift movement in New Caledonia – Loyalty Islands area and their plate tectonics interpretation, *Tectonophys.,* **24,** 133–150.

Duncan, R. A. & McDougall, I., 1976. Linear volcanism in French Polynesia, *J. Volcanol. Geotherm. Res.,* **1,** 197–227.

Francheteau, J., 1983. The oceanic crust, *Sci. Am.,* **249,** 114–129.

Herron, E. M., 1972. Sea-floor spreading and the Cenozoic history of the East–Central Pacific, *Bull. geol. Soc. Am.,* **83,** 1671–1692.

Jarrard, R. & Clague, D. A., 1977. Implications of Pacific islands and seamounts ages for the origin of volcanic chains, *Rev. Geophys. Space Phys.,* **15,** 57–76.

Johnson, R. H., 1980. Seamounts in the Austral Islands region, *Natn. geogr. Soc. Res. Repts.,* **12,** 389–405.

Lacey, A., Ockendon, J. R. & Turcotte, D. L., 1981. On the geometrical forms of volcanoes, *Earth planet. Sci. Lett.,* **54,** 139–143.

Lambeck, K., 1981. Lithospheric response to volcanic loading in the Southern Cook Islands, *Earth planet. Sci. Lett.,* **55,** 482–496.

Lambeck, K. & Coleman, R., 1982. A search for seamounts in the Southern Cook and Austral region, *Geophys. Res. Lett.,* **9,** 389–392.

Lame, D. B. & Born, G. H., 1982. SEASAT measurement system evolution: achievements and limitations, *J. geophys. Res.,* **87,** 3175–3188.

Lameyre, J., Black, R., Bonin, B. & Giret, A., 1984. Les provinces magmatiques de l'Est américain, de l'Ouest africain et des Kerguelen. Indications d'un contrôle tectonique et d'une initiation superficielle du magmatisme intraplaque et des processus associés, *Annls. Soc. Géol. N.,* **C11,** 101–116.

Lazarewicz, A. P. & Schwank, D. C., 1982. Detection of uncharted seamounts using satellite altimetry, *Geophys. Res. Lett.,* 9, 385–388.

Mammerickx, J., Smith, S. M., Taylor, I. L. & Chase, T. E., 1975. *Topography of the South Pacific Map,* Scripps Inst. Oceanogr., Univ. of Calif., San Diego, La Jolla.

McDougall, I. & Duncan, R. A., 1980. Linear volcanic chains recording plate motion? *Tectonophys.,* 63, 275–295.

McNutt, M. K., 1984. Lithospheric flexure and thermal anomalies, *J. geophys. Res.,* 89, 11 180–11 194.

Morgan, W. J., 1972. Deep mantle convection plumes and plate motions, *Bull. Am. Ass. Petrol. Geol.,* 56, 203–213.

Okal, E. A. & Cazenave, A., 1985. A model for the plate tectonic evolution of the East–Central Pacific based on SEASAT investigations, *Earth planet Sci. Lett.,* 72, 99–116.

Parker, R. L., 1972. The rapid calculation of potential anomalies, *Geophys. J. R. astr. Soc.,* 31, 447–455.

Pontoise, B., Baudry, N., Diament, M., Aubouin, J., Blanchet, R., Butscher, J., Chotin, P., Dupont, J., Eissen, J-P., Ferrière, J., Herzer, R., Lapouille, A., Louat, R., D'Ozouville, L., Pelletier, B., Soakai, S. & Stevenson, A., 1987. Levés SEABEAM dans l'archipel des Iles Australes: confirmation d'une nouvelle méthode de localisation de monts sous-marins basée sur l'analyse des données SEASAT, *C. r. Acad. Sci., Paris,* in press.

Reigber, C., Balmino, G., Moynot, B. & Mueller, H., 1983. The GRIM 3 earth gravity field model, *Mar. Geodesy,* 8, 93–138.

Sailor, R. V. & Okal, E. A., 1983. Application of SEASAT altimeter data in seismotectonic studies of the South Central Pacific, *J. geophys. Res.,* 88, 1572–1580.

Sandwell, D. T., 1984a. A detailed view of the South Pacific geoid from satellite altimetry, *J. geophys. Res.,* 89, 1089–1104.

Sandwell, D. T., 1984b. *Along-track deflection of the vertical from SEASAT: GEBCO overlays,* NOAA Technical Memorandum NOS NGS-40.

Sclater, J. G., Jaupart, C. & Galson, D., 1980. The heat flow through oceanic and continental crust and the heat loss of the Earth, *J. geophys. Res.,* 18, 269–311.

Summerhayes, D. P., 1967. Bathymetry and topographic lineation in the Cook Islands, *N. Z. J. Geol. Geophys.,* 10, 1382–1398.

Ten Brink, U. S. & Watts, A. B., 1985. Seismic stratigraphy and the flexural moat flanking the Hawaiian Islands, *Nature,* 317, 421–424.

Walcott, R. I., 1970. Flexure of the lithosphere at Hawaii, *Tectonophys.,* 9, 435–446.

Watts, A. B., 1978. An analysis of isostasy in the world oceans, 1 – Hawaiian–Emperor seamount chain, *J. geophys. Res.,* 83, 5985–6004.

Watts, A. B. & Cochran, J. R., 1974. Gravity anomalies and flexure of the lithosphere along the Hawaiian–Emperor seamount chain, *Geophys. J. R. astr. Soc.,* 38, 119–141.

Watts, A. B. & Ribe, N. M., 1984. On the geoid heights and flexure of the lithosphere at seamounts, *J. Geophys. Res.,* 89, 11 152–11 170.

Watts, A. B., Cochran, J. R. & Selzer, G., 1975. Gravity anomalies and flexure of the lithosphere: a three-dimensional study of the great Meteor seamount, Northeast Atlantic, *J. geophys. Res.,* 80, 1391–1398.

Watts, A. B., Cochran, J. R., Patriat, P. & Doucoure, M., 1985a. A bathymetry and altimetry profile across the Southwest Indian ridge crest at 31°S latitude, *Earth planet. Sci. Lett.,* 73, 129–139.

Watts, A. B., Ten Brink, U. S., Buhl, P. & Brocher, T. M., 1985b. A multichannel seismic study of lithospheric flexure across the Hawaiian–Emperor seamount chain, *Nature,* 315, 105–111.

White, J. V., Sailor, R. V., Lazarewicz, A. R. & Le Schack, A. R., 1983. Detection of seamount signature in SEASAT altimeter data using matched filters, *J. geophys. Res.,* 88, 1541–1551.

Woollard, G. P., 1975. The interrelationships of crustal and upper mantle parameter values in the Pacific, *Rev. Geophys. Space Phys.,* 13, 87–137.